Linear elastic properties derivation from microstructures representative of transport parameters

Minh Tan Hoang, Guy Bonnet, Hoang Tuan Luu, Camille Perrot

Linear elastic properties derivation from microstructures representative of transport parameters

M. T. Hoang[1, 2], G. Bonnet[1], H. T. Luu[1], C. Perrot[1]

1: Université Paris-Est, Laboratoire Modélisation et Simulation Multi Echelle, MSME UMR 8208 CNRS, 5 Bd Descartes, 77454 Marne-la-Vallée, France

2: Faurecia Interior Systems, Acoustic TechCenter, Z.I. François Sommer BP 13, 08210 Mouzon, France

Abstract: Can a periodic unit cell (PUC), whose local characteristic lengths have been identified as governing compressional sound wave properties in solid foams, provide a basis to model their linear elastic properties? How do elastic properties depend on membranes or solid films which may partially close the interconnections between the pores of solid foams? These two questions are the basis of the paper. A positive answer to the first question leads to foam microstructures with a full set of macroscopic parameters entering into the Biot-Allard poroelastic equations, which are critical for the sound insulation problem. Contributing factors such as membrane content, and thickness, are shown to have a significant effect on mechanical properties such as Young's modulus and Poisson ratio. Acoustical properties including sound transmission loss calculations and measurements indicate that this multi-scale approach is a reliable and insofar promising first attempt to bridge the gap between microstructure and the long-wavelength full acoustic properties (visco-inertial, thermal, elastic) of real poroelastic materials.

Keywords: unit-cell, scaling, transport parameters, membrane effect, elastic properties, poro-elasticity, unified approach.

1. Introduction

A main original standpoint of our study is the combination of the identification of local characteristic lengths governing sound wave properties in solid foams [1] with linear elastic property simulations by applying a version of periodic homogenization method [2] in the presence of polyhedral unit cells with cubic symmetry (namely non-elongated Kelvin cell models). Fluid-flow and heat transfer simulations in three-dimensional periodic unit cells of solid foams lead to the formation of structured materials with essentially two local characteristic lengths, the pore and throat sizes [3-4]; Fig. 1. Importantly, the introduction of solid films or membranes at the interconnection between pores that partially close them allows the capturing of visco-inertial and thermal dissipation mechanisms in a consistent way at both micro and macro scales.

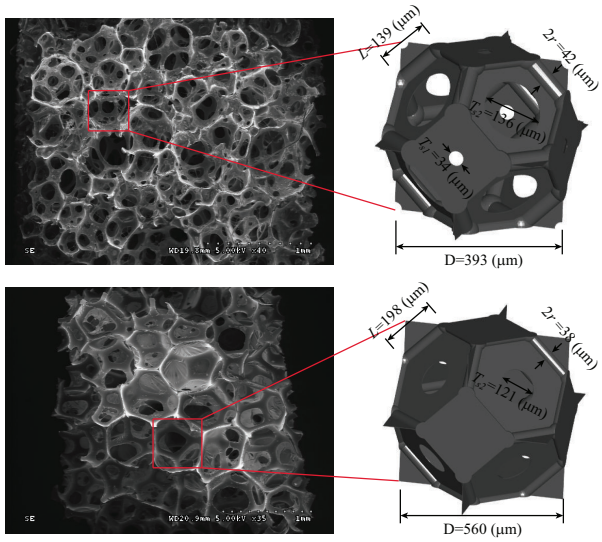

Figure 1: Geometrical characteristics of two different solid foam samples, H1 (top) and H2 (bottom).

The resultant bicontinuous structure is supposed to be non-deformable at first, allowing for the identification of the PUC local characteristic lengths. Then, by using as the unit cell a representative volume which is compatible with the visco-inertial and thermal response, the linear elastic properties of the generated structures can be studied. Using a finite element based micromechanics procedure, we calculate the elastic properties of unit cells obtained by simulated visco-thermal dissipations. This strategy is distinguished from other micromechanical methods which take into account the presence of membranes [5-9]. Indeed, these previous works use fully opened or fully closed cells.

2. Microporoelastic analysis

2.1 Elastic stiffnesses and compliances

With respect to a fixed coordinate system $x_1 = x_2 = x_3$, let σ_{ij} and ε_{ij} be the stresses and strains, respectively, in an anisotropic elastic material. The stress-strain law can be written as

$$\sigma_{ij} = C_{ijks}\, \varepsilon_{ks}, \qquad [1]$$

in which C_{ijks} are the elastic stiffness coefficients which are components of a fourth rank tensor. They

satisfy symmetry conditions. The inverse of this relation is written as

$\varepsilon_{ij} = S_{ijks}\,\sigma_{ks}$, [2]

where S_{ijks} are the elastic compliances which are components of a fourth rank tensor. They possess the same symmetry conditions as the stiffness tensor.

2.2 Contracted notations

Introducing the contracted notation (Voigt, 1910) the stress-strain law [1] can be written as

$\sigma_i = c_{ij}\,\varepsilon_j$, $c_{ij} = c_{ji}$ [3]

In other words, due to the symmetry ($\sigma_{ij} = \sigma_{ji}$, and $\varepsilon_{ij} = \varepsilon_{ji}$), only six independent components can appear in the stress and strain tensors. These six independent components of stress and strain can be "contracted" to a single index notation by writing:

$\sigma_{ij} = \sigma_k$, $\varepsilon_{ij} = \varepsilon_k$; [4]

and using, for the substitution $(i, j) \rightarrow k$, the rule, (1,1) $\rightarrow$1, (2,2)$\rightarrow$2, (3,3)$\rightarrow$3, (2,3) and (3, 2) $\rightarrow$ 4, (1,3) and (3,1) $\rightarrow$ 5, (1,2) and (2,1) $\rightarrow$ 6. As a consequence, the fourth order elastic constant tensor may be contracted to a two-index notation by the application of the following conventions:

$$\underline{\underline{\sigma}} \rightarrow \underset{\sim}{\sigma} := \begin{pmatrix} \sigma_{11} \\ \sigma_{22} \\ \sigma_{33} \\ \sqrt{2}\sigma_{23} \\ \sqrt{2}\sigma_{31} \\ \sqrt{2}\sigma_{12} \end{pmatrix}, \text{ and } \underline{\underline{\varepsilon}} \rightarrow \underset{\sim}{\varepsilon} := \begin{pmatrix} \varepsilon_{11} \\ \varepsilon_{22} \\ \varepsilon_{33} \\ \sqrt{2}\varepsilon_{23} \\ \sqrt{2}\varepsilon_{31} \\ \sqrt{2}\varepsilon_{12} \end{pmatrix}; \quad [5]$$

the factor of $\sqrt{2}$ being inserted in order that the equality $\underline{\underline{\sigma}} : \underline{\underline{\varepsilon}} = \underset{\sim}{\sigma}.\underset{\sim}{\varepsilon}$ holds true. Following this convention, the generalized Hooke's law relationship between the elements of the stress and strain tensor (represented as six element column vectors) can be compactly written in matrix notations as

$\underset{\sim}{\sigma} = \underset{\approx}{c}.\underset{\sim}{\varepsilon}$, [6]

where $\underset{\approx}{c}$ is a six-by-six symmetric matrix. An expanded form of the matrix notation is given below:

$$\begin{pmatrix} \sigma_{11} \\ \sigma_{22} \\ \sigma_{33} \\ \sqrt{2}\sigma_{23} \\ \sqrt{2}\sigma_{31} \\ \sqrt{2}\sigma_{12} \end{pmatrix} = \begin{pmatrix} c_{11} & c_{12} & c_{13} & c_{14} & c_{15} & c_{16} \\ & c_{22} & c_{23} & c_{24} & c_{25} & c_{26} \\ & & c_{33} & c_{34} & c_{35} & c_{36} \\ & sym & & c_{44} & c_{45} & c_{46} \\ & & & & c_{55} & c_{56} \\ & & & & & c_{66} \end{pmatrix} \begin{pmatrix} \varepsilon_{11} \\ \varepsilon_{22} \\ \varepsilon_{33} \\ \sqrt{2}\varepsilon_{23} \\ \sqrt{2}\varepsilon_{31} \\ \sqrt{2}\varepsilon_{12} \end{pmatrix}. \quad [7]$$

As indicated previously, it is frequently useful to express the strain in terms of the stress,

$\underset{\sim}{\varepsilon} = \underset{\approx}{s}.\underset{\sim}{\sigma}$, [8]

where $\underset{\approx}{s}$ is the compliance tensor made of the 21 independent elements s_{ij}. The quantity $\underset{\approx}{s}$ is the inverse of $\underset{\approx}{c}$ in the matrix sense $\underset{\approx}{s} = \underset{\approx}{c}^{-1}$. The twenty-one coefficients, s_{ij}, are called the compliance constants.

2.3 Material symmetries

This paper addresses the linear elastic properties of partially closed cell solid foams with membrane-based tetrakaidecahedral cellular morphologies. This geometry exhibits a cubic symmetry. In this case, the elasticity tensor is defined by three independent coefficients, the elastic stiffnesses:

$$C^{cubic} = \begin{pmatrix} C_{11} & C_{12} & C_{12} & 0 & 0 & 0 \\ & C_{11} & C_{12} & 0 & 0 & 0 \\ & & C_{11} & 0 & 0 & 0 \\ & & & C_{44} & 0 & 0 \\ & sym & & & C_{44} & 0 \\ & & & & & C_{44} \end{pmatrix}. \quad [9]$$

Consequently, the elastic behavior can be described based on only three independent elastic parameters e.g. C_{11}, C_{12}, C_{44}. Alternatively, the elastic compliances S_{ij} might be expressed in terms of the elastic stiffnesses:

$$\begin{cases} S_{11} = S_{22} = S_{33} = \dfrac{C_{11} + C_{12}}{C_{11}^2 + C_{11}C_{12} - 2C_{12}^2}, \\ S_{12} = S_{21} = S_{13} = S_{31} = S_{23} = S_{32} = \dfrac{-C_{12}}{C_{11}^2 + C_{11}C_{12} - 2C_{12}^2}, \\ S_{44} = S_{55} = S_{66} = \dfrac{1}{C_{44}}. \end{cases} \quad [10]$$ [4]

Attention will be directed in the next sections to (1) the specification of two kinds of numerical experiments required to completely characterize the elastic compliances and stiffnesses in terms of the base material's properties and to (2) the obtention of averaged (i) transversely isotropic properties or (ii) isotropic properties obtained from the results of the numerical experiments.

2.4 Numerical experiments

A simple tensile numerical experiment is such that σ_{11} is different from zero and all other loads deleted. Under these loading conditions, the relationship $\underset{\sim}{\varepsilon} = \underset{\approx}{S}\underset{\sim}{\sigma}$ greatly simplifies to yield

$$\begin{cases} \varepsilon_{11} = S_{11}\sigma_{11}, \\ \varepsilon_{22} = S_{12}\sigma_{11}, \\ \varepsilon_{33} = S_{13}\sigma_{11}, \\ \varepsilon_{23} = \varepsilon_{31} = \varepsilon_{12} = 0. \end{cases} \quad [11]$$

The longitudinal elastic modulus and Poisson ratios were deduced by definition:

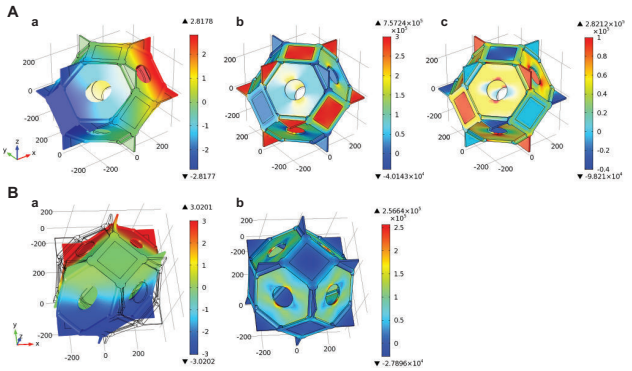

Fig. 2: Numerical experiments allowing identification of the elastic constants (illustrated with sample H_2).

$$\begin{cases} E_L = \dfrac{\sigma_{11}}{\varepsilon_{11}} = \dfrac{1}{S_{11}}, \\ \nu_{12} = \dfrac{\varepsilon_{22}}{\varepsilon_{11}} = -\dfrac{S_{12}}{S_{11}}, \\ \nu_{13} = \dfrac{\varepsilon_{33}}{\varepsilon_{11}} = -\dfrac{S_{13}}{S_{11}}. \end{cases} \quad [12]$$

For materials with cubic symmetry, substituting the expressions in [10] into equation [12] leads to

$$\begin{cases} E_L = \dfrac{C_{11}^2 + C_{11}C_{12} - 2C_{12}^2}{C_{11} + C_{12}}, \\ \nu_{12} = \nu_{13} = \dfrac{C_{12}}{C_{11} + C_{12}}, \end{cases} \quad [13]$$

which relates the longitudinal modulus and Poisson ratios to the elastic constants.

To calculate the macroscopic elastic constants of materials a macroscopic strain is applied to the unit cell (Fig. 2). The displacement field inside the cell is the solution of the cell problem obtained from the homogenization of periodic media.

It is given by:

$$\mathbf{u} = \boldsymbol{E}.\mathbf{x} + \mathbf{u}_{\mathbf{per}} \ , \quad [14]$$

where $\mathbf{u}_{\mathbf{per}}$ complies with periodicity conditions on the cell boundary. It can be shown [10] that, accounting for the symmetries of the cell, these periodicity conditions can be changed into mixed boundary conditions enforcing that some components of $\mathbf{u}$ are equal to the similar components of $\boldsymbol{E}.\mathbf{x}$, while expressing that the other components of the traction vector are null. For further details the reader is referred to Sec. 4.2.1 of Ref. [11] from J.C. Michel *et al.* entitled "Symmetry conditions" and in Appendix A of the same paper.

The components of the macroscopic effective stress tensor $\underset{\sim}{\Sigma}$ induced by the macroscopic strain $\boldsymbol{E}$ are obtained by averaging the local stress tensor $\underset{\sim}{\sigma}$ obtained after solving the cell problem,

$$\underset{\sim}{\Sigma} = \left\langle \underset{\sim}{\sigma} \right\rangle_V = \frac{1}{V}\int_V \sigma dV \ . \quad [15]$$

But, from another point of view, the macroscopic stress tensor is related to the macroscopic strain tensor by,

$$\forall \underset{\sim}{E}, \qquad \underset{\sim}{\Sigma} = \left\langle \underset{\sim}{\sigma} \right\rangle_V = \underset{\sim}{C}.\underset{\sim}{E} \ . \quad [16]$$

This computation produces therefore some components of the elasticity tensor.

For the materials with cubic symmetry which contain only three independent elastic coefficients, only two numerical experiments are required to find out completely the elasticity matrix, one by using a macroscopic tensile strain and another one by using a macroscopic shear strain.

In a first step we pay attention to a tensile strain numerical experiment (Fig. 2) for which we impose a uniform macroscopic strain, $E = E_{11}\mathbf{e}_1 \otimes \mathbf{e}_1$, from which two elastic constants are found from the macroscopic stress tensor:

$$\begin{cases} C_{11} = \Sigma_{11}/E_{11}, \\ C_{12} = \Sigma_{22}/E_{11}. \end{cases} \quad [17]$$

In a second step, we impose a uniform macroscopic strain $E = E_{12}\left(\mathbf{e}_1 \otimes \mathbf{e}_2 + \mathbf{e}_2 \otimes \mathbf{e}_1\right)$ to model a shear strain numerical experiment. This leads to

$$C_{44} = \Sigma_{12}/E_{12} \quad . \quad [18]$$

This completes the elasticity tensor.

2.5 Macroscopically transversely isotropic and isotropic material configurations

The cubic cell used previously has been built by using some properties of the local geometry. However, the real material seen in Fig. 1 presents cells which are similar with the cubic cell, but whose shape and orientation departs from regularly aligned cells. In practice, real foams display either transversely isotropic properties (with a rotational symmetry axis along the growth direction of the fibers) or fully isotropic properties.

The properties of an equivalent isotropic material can be built on the basis of the cubic cell by considering that the real material is made of cubic cells which have an arbitrary orientation. It can be obtained by computing the elasticity tensor $S'_{ij}(\psi,\theta,\varphi)$ for an arbitrary orientation of the axes of the cell, using the usual axes transformation of a tensor, and by averaging these properties over all orientations, i.e. on all possible Euler angles (ψ,θ,φ). This leads to an upper bound of the compliance tensor and to a lower bound of the elasticity tensor,

Foam	Method	ϕ	Λ' (μm)	k_0 ($\times 10^{-10}$ m^2)	Λ (μm)	α_∞	k_0' ($\times 10^{-10}$ m^2)
H_1	Computation	0.93 ± 0.01	146 ± 22	5.35 ± 0.42	55 ± 6	1.40 ± 0.26	28 ± 12
	Measurements						
	Characterization		143 ± 57		33 ± 4	1.05 ± 0.08	55 ± 28
H_2	Computation	0.97 ± 0.01	179 ± 46	2.56 ± 0.60	53 ± 9	2.40 ± 0.55	48 ± 26
	Measurements						
	Characterization		424 ± 92		13 ± 6	1.58 ± 0.64	53 ± 16

Table 1. Macroscopic parameters: comparison between computational and experimental results.

$$S_{ij}^{I} = \frac{1}{8\pi^2} \int_0^{2\pi} \int_0^{\pi} \int_0^{2\pi} S_{ij}^{'}(\psi,\theta,\varphi) \sin\theta d\psi d\theta d\varphi \ . \qquad [19]$$

This produces finally a relationship between the lower bound of the components of the equivalent isotropic tensor S_{ij}^{I} and those of the elastic properties of the cubic material.

$$\begin{cases} S_{11}^{I} = S_{22}^{I} = S_{33}^{I} = \dfrac{3S_{11} + 2S_{12} + 2S_{44}}{5}, \\ S_{12}^{I} = S_{21}^{I} = S_{13}^{I} = S_{31}^{I} = S_{23}^{I} = S_{32}^{I} = \dfrac{S_{11} + 4S_{12} - S_{44}}{5}, \\ S_{44}^{I} = S_{55}^{I} = S_{66}^{I} = \dfrac{2S_{11} - 2S_{12} + 3S_{44}}{5}. \end{cases} \qquad [20]$$

For a transversely isotropic material, the computation is the same, but by restricting the orientation of the axes to the ones perpendicular to the growth direction, i.e. by averaging over only all values of θ:

$$S_{ij}^{TI} = \frac{2}{\pi} \int_0^{\pi/2} S_{ij}^{'}(\theta) d\theta \ . \qquad [21]$$

This produces finally an upper bound of the components of the compliance tensor, which possess the properties of a transversely isotropic tensor, including $S_{22} - S_{23} = S_{44}$:

$$\begin{cases} S_{11}^{TI} = S_{11}, \\ S_{22}^{TI} = S_{33}^{TI} = \dfrac{3S_{11} + S_{12} + S_{44}}{4}, \\ S_{44}^{TI} = \dfrac{S_{11} - S_{12} + S_{44}}{2}, \\ S_{55}^{TI} = S_{66}^{TI} = S_{44}, \\ S_{12}^{TI} = S_{21}^{TI} = S_{13}^{TI} = S_{31}^{TI} = S_{12}, \\ S_{23}^{TI} = S_{32}^{TI} = \dfrac{3S_{12} + S_{11} - S_{44}}{4}, \\ S_{24}^{TI} = S_{42}^{TI} = 0, \\ S_{34}^{TI} = S_{43}^{TI} = 0. \end{cases} \qquad [22]$$

3. Results and discussion

3.1 Geometrical and transport macroscopic properties

Before looking at the mechanical results, it is of interest to consider the purely geometrical macroscopic properties (ϕ, Λ') and transport parameters (k_0, Λ, α_∞) which were obtained on the cubic cell.

The porosity ϕ was measured with a reasonable accuracy from the missing mass method [12]. The permeability k_0 was also directly measured as in Stinson and Daigle [13], after having removed a film at the surface of foam sample H_1 whose presence is due to the injection process. Then, the determination of the missing parameters, Λ', Λ, α_∞, and k_0' is based on an inverse procedure [14-15] using an analytical inversion from standing wave tube measurements [16] and Johnson-Champoux-Allard-Lafarge [17-19] model.

The purely geometrical macroscopic properties (Λ') and transport parameters ($\Lambda, \alpha_\infty, k_0'$) computed from the course of this multi-scale approach are in a rather good agreement with experimental data (Λ', Λ, α_∞, k_0'), especially when standard deviations are taken into account as seen in Table 1.

Considering the experimental characterization as the ground truth, one might however estimate the coefficients Λ to be slightly overestimated by the local geometry model, which occurs for idealized unit cells with monodisperse throat sizes. Indeed, computed and measured values are of similar magnitude for the H_1 foam sample (32% of relative difference), whereas for the H_2 foam sample a factor of two is observed (116% of relative difference). Because the viscous characteristic length was determined for a periodic unit cell with a single closure rate of membranes, the later model is insensitive to polydispersity of the throat sizes. More complex structures that contain, for example, additional throats of very small sizes could be used to extend this analysis. In agreement with this explanation, a microstructure analysis from SEM images is conducted in the next section, confirming that the overestimation of Λ calculation was due to the fact that the model ignores the presence of many very small wholes inside membranes. Together with a relatively close match between the measured and computed macroscopic parameters ($\Lambda', \alpha_\infty, k_0'$), this analysis about the origin of Λ small discrepancies and the microstructural results below indicate that the local geometry models presented in Fig. 1 capture the essential physics of the transport phenomena inside the foams.

3.2 Linear elastic properties

The basic ingredients of flexible urethane foams of the type considered in this study are ester resin (or polyol), diisocyanate, water, catalysts and surfactants. [20] Foam H_1 was manufactured from the standpoint of these typical ingredients with a view of lowering significantly the Young's modulus of the resulting porous material when compared to standard plastic foams, and foam H_2 is a commercial product. The samples represent cylindrical subsections of large panels of diameter equal to 44.5 mm. Their heights are equal to 25 mm for H_1; and 10 mm, 15 mm, and 20 mm for H_2.

Accurate literature values for the microscopic Young's modulus E_μ and Poisson ratio ν_μ are not available because these values are depending on processing strategy. The values obtained in the literature for E_μ are scattered within a range of more than one order of magnitude, they are typically lying between 2 and 30 MPa. [21] By contrast, the microscopic Poisson ratio seems relatively stable, with $\nu_\mu \simeq 0.25$. As mentioned by Gong et *al.* [5], some foam chemists believe that the polymer flow resulting from the foaming process may cause preferential alignment of the long molecules of the material along the ligaments. Since these characteristics may not be easily achievable in bulk material, they recommend that the mechanical properties of the polymer be measured directly from foam ligaments. Therefore, the main conclusion which can be drawn is that specific measurements should be made on the material. Microscopic Young's modulus was estimated from Mercury Intrusion Porosimetry (MIP) for foam sample H_1, yielding $E_\mu \simeq 7.07 \pm 1.18$ MPa. This method failed at estimating the microscopic Young's modulus of foam sample H_2, presumably because foam sample H_2 may also contain an occluded porosity, which prevents mercury to saturate all of the fluid phase, and renders experimental data difficult to interpret. Without these complete measurements at the present time, the base material of foam sample H_2, which must have a higher Young's modulus than the base material of foam sample H_1, is characterized by $E_\mu \simeq 25$ MPa, this value being justified in the following.

From the above analysis it can be concluded that because of the strong dependence of the foam properties on the base material, it is better to replace all results of the computations performed along the lines of the previous section by non-dimensional values; for instance $E_I^{nd} = E_I / E_\mu$. These non-dimensional data were first computed with membranes. A parameter which has a strong effect on the results is the membrane thickness. An estimate of the membrane thickness $t \simeq 1.7 \pm 0.4$ μm was obtained by scanning electron micrographs. Two simulations were carried out: with and without membranes. The characterization results of elastic parameters carried out at macro-scale from quasi-static compressional experiments [22-23] are given in Table 2 (left). For comparison with the static computed results, the relative Young's moduli of both foams are given for ultimate values of E_μ (2-30MPa), Table 2. These values can be compared on the same table with relative macroscopic Young's moduli coming from the computations. Not that frequency-dependent characterization results were deliberately not presented in this paper, because of the static nature of the proposed computational approach.

Foam	$1000E_{exp}$ (Pa)	$1000E_{exp}/E_{\mu(min)}$ (-)	$1000E_{exp}/E_{\mu(max)}$ (-)	$1000E_{comp}/E_\mu$ (with membranes)	$1000E_{comp}/E_\mu$ (without membranes)
H_1	14.02	7.01	0.46	8.43	4.79
H_2	11.93	5.96	0.40	4.73	0.71

Table 2. Comparison between measured E_{exp} and computed E_{comp} elastic Young's moduli for a membrane thickness value t equal to 1.7 μm.

Obviously, the range of the experimental relative moduli E_{exp}/E_μ follows the one of the polyurethane base material modulus E_μ. However, some conclusions can still be drawn. It can be seen for H_1 that the estimation of the relative modulus with membranes is not far from the experimental one, providing that the Young's modulus of the base material is in the vicinity of the smallest values available in the literature (this is rather consistent with previously mentioned estimates of the microscopic Young's modulus obtained by MIP). For H_2 foam sample, the value of the relative Young's modulus obtained with membranes is clearly inside the admissible range of relative moduli, within the higher values so that the Young's modulus of the base material must also be relatively low. From the above examples it can be concluded that membranes must be modeled when the goal is to determine the homogenized linear elastic properties for foams containing a high closure rate of membranes.

4. Conclusion

Let us have an overall view of the results that were derived from this multi-scale approach with the poroelastic foam samples used in this paper (Fig. 1). For the sake of clarity, let us recall the procedure. The porosity ϕ, permeability k_0 and ligament length L are assumed to be known from measurements. In the multi-scale approach, the extension of the solid film constituting the membranes was implemented at growing rates. The cell size is known from SEM experiments and the closure rate of membranes is

adjusted for obtaining the experimental permeability. Macroscopic parameters are then computed from numerical homogenization and compared to the values that were measured at macro-scale in Sec. 3 and gathered in Table 1. These later values serve in a sense as bridges between microstructure and acoustical macro-behavior with microphysical and micromechanical foundations. The numerical simulations are generally in good agreement with the standing wave tube measured values. As also shown above the proposed micromechanical method can provide reasonable estimates of linear elastic properties for poroelastic foams including the significant effects of membranes' closure rate and thickness. The method is an idealized periodic cell one, based on the use of a simplified cellular morphology with identified local characteristic lengths. Further systematic investigation on the sensitivity of the results with regard to choice of particular features of the cellular morphology should be carried out. It is noted that accurate values for the Young's modulus and Poisson ratio of the base material are difficult to obtain because of the variability of the base material itself encountered in the foaming process and the need to implement advanced characterization techniques at this scale. In other words extending this multi-scale method to real life sound insulation optimization problems is not straightforward but the present methodology should readily be extended.

5. Acknowledgement

The authors thank ANRT and Faurecia company for financial support (CIFRE No. 748/2009). Partial support for this work was also provided by Université Paris-Est (mobility grant from the ED SIE) and Université Paris-Est Marne-la-Vallée (BQR No. FG 354/2009). We acknowledge M. Vandamme (Laboratoire Navier, Université Paris-Est) and H. T. Luu (MSME, Université Paris-Est) for the application of MIP in measuring microscopic Young's modulus; R. Combes (LGE, Université Paris-Est) and H. T. Luu for membrane thickness estimates through SEM imaging; T. Niemeyer for compression testing together with L. Bischoff, and A. Duval, J.-F. Rondeau for helpful input and fruitful discussions (Faurecia); S. Gutierrez for SEM imaging at low magnifications of the solid foam samples (CCM, Université de Sherbrooke); R. Panneton for providing the in house FE axisymmetric poroelastic formulation and for subsequent stimulating exchanges; and F. Chevillote for discussions about data analysis (Matelys).

6. References

[1] M. T. Hoang and C. Perrot: "*Identifying local characteristic lengths governing sound wave properties in solid foams* ", J. Appl. Phys., 113, 084905, AIP, 2013.

[2] M. Bornert, T. Bretheau, P. Gilormini: "*Homogenization in mechanics of materials*", 448 pages, ISTE Publishing Company, 2006.

[3] C. Perrot, F. Chevillotte, M. T. Hoang, G. Bonnet, F.-X. Bécot, L. Gautron, and A. Duval: "*Microstructure, transport, and acoustic properties of open-cell foam samples: Experiments and three-dimensional numerical simulations* ", J. Appl. Phys., 111, 014911, AIP, 2012.

[4] M. T. Hoang and C. Perrot: "*Solid films and transports in cellular foams* ", J. Appl. Phys., 112, 054911, AIP, 2012.

[5] L. Gong, S. Kyriakides, W.-Y. Jang, "Compressive response of open-cell foams. Part I: Morphology and elastic properties", Int. J. Solids Struct., 42, 1355, Elsevier, 2005.

[6] R. M. Sullivan, L. J. Ghosn, B. A. Lerch, "A general tetrakaidecahedron model for open-celled foams", Int. J. Solids Struct., 45, 1754, Elsevier, 2008.

[7] R. M. Sullivan, L. J. Ghosn, B. A. Lerch, E. H. Baker, "Elongated Tetrakaidecahedron micromechanics model for space shuttle external tank foams", NASA Technical Reports Server (NTRS), 215137, NASA Center for AeroSpace Information (CASI), 2009.

[8] W.-Y. Jang, S. Kyriakides, A. M. Kraynik, "On the compressive strength of open-cell metal foams with Kelvin and random cell structures", Int. J. Solids Struct., 47, 2872, Elsevier, 2010.

[9] P. Thiyagasundaram, B. V. Sankar, N. K. Arakere, "Elastic properties of open-cell foams with tetrakaidecahedral cells using finite element analysis", AIAA Journal, 48, 818, AIAA, 2010.

[10] "Homogenization in mechanics of materials", Edited by M. Bornert, T. Bretheau, P. Gilormini (ISTE Publishing Company), 448 pages (2006).

[11] J.C. Michel, H. Moulinec and P. Suquet, "Effective properties of composite materials with periodic microstructure: a computational approach", Comput. Methods Appl. Mech. Engrg. 172, 109 (1999).

[12] R. Panneton and E. Gros, "A missing mass method to measure the open porosity of porous solids", Acta Acustica United With Acustica 91, 342 (2005).

[13] M. R. Stinson and G. A. Daigle, "Electronic system for the measurement of flow resistance", J. Acoust. Soc. Am. 83, 2422 (1988).

[14] R. Panneton, X. Olny, "Acoustical determination of the parameters governing viscous dissipation in porous media", J. Acoust. Soc. Am. **119**, 2027 (2006)

[15] X. Olny, R. Panneton, "Acoustical determination of the parameters governing thermal dissipation in porous media", J. Acoust. Soc. Am. **123**, 814 (2008).

[16] H. Utsuno, T. Tanaka, T. Fujikawa, and A. F. Seybert, "Transfer function method for measuring characteristic impedance and propagation constant of porous materials", J. Acoust. Soc. Am. **86**, 637 (1989).

[17] D. L. Johnson, J. Koplik, and R. Dashen, “Theory of dynamic permeability and tortuosity in fluid-saturated porous media”, J. Fluid Mech. 176, 379 (1987).

[18] Y. Champoux and J. F. Allard, “Dynamic tortuosity and bulk modulus in air-saturated porous media”, J. Appl. Phys. 70, 1975 (1991).

[19] D. Lafarge, P. Lemarinier, J. F. Allard, V. Tarnow, “Dynamic compressibility of air in porous structures at audible frequencies”, J. Acoust. Soc. Am. 102, 1995 (1997).

[20] L.D. Artavia and C.W. Macosko, “Polyurethane flexible foam formation”, (pp. 22–55); R.D. Priester and R. B. Turner, “The morphology of flexible polyurethane matrix polymers”, (pp. 78-103); in Low density cellular plastics: physical basis of behavior, Edited by N.C. Hilyard and A. Cunningham (Chapman & Hall, London, 1994).

[21] J. Lecomte-Beckers, “Cours de physique des matériaux : Partie Polymères ” (Université de Liège, 2009), Chap. 8, pp. 7. English translation : Lecture notes on physics of materials, http://www.metaux.ulg.ac.be/Fichierpourtelech/polym/ch%208.pdf (date last viewed 11/14/12).

[22] E. Mariez, S. Sahraoui, and J. F. Allard, “Elastic constants of polyurethane foam’s skeleton for Biot model”, Proceedings of Internoise 96, pp. 951–954 (1996).

[23] C. Langlois, R. Panneton and N. Atalla, “Polynomial relations for quasi-static mechanical characterization of isotropic poroelastic materials”, J. Acoust. Soc. Am. 110, 3032 (2001).